I S A V

Journal of Theoretical and Applied Vibration and Acoustics

journal homepage: http://tava.isav.ir

Fault detection of rolling element bearing using a temporal signal with artificial intelligence techniques

Mahdi Behzad[a,*], **Hassan Izanlo**[a], **Ali Davoodabadi**[a], **HessamAddin Arghand**[b]

[a] *School of Mechanical Engineering, Sharif University of Technology, Tehran, Iran*

[b] *Engineering Department, University of Zanjan, Zanjan, Iran*

ARTICLE INFO

Article history:
Received 28 February 2021

Received in revised form
19 June 2021

Accepted 29 June 2021

Available online 18 July 2021

Keywords:
Fault detection

rolling-element bearing

convolutional neural network

feed-forward neural network

detection of impact

ABSTRACT

Fault detection of rolling element bearing (REB), has a very effective role in increasing the reliability of machinery and improving future decisions for rotating machinery operation. In this study, a new method based on a convolutional neural network (CNN) is developed for fault detection of REB. Its performance will be compared with other artificial intelligence (AI) techniques, 2-layer, and deep feedforward neural network (FFNN). In this regard, a set of accelerated-life tests has been implemented on an experimental platform. The models are aimed to recognize the impact pattern in the raw signals generated by faulty REBs. The innovation of the present study is to convert the high-dimensional input as a raw temporal signal to low-dimensional output. The developed method does not need preprocessing of data. Using several types of accelerated tests prevents overfitting. The result shows that the accuracy of the developed CNN-based method is 98.6% for all data sets and 94.6% for the validation dataset. The accuracy of the 2-layer FFNN is 85% for all datasets and 74.2% for the validation dataset and the accuracy of the deep FFNN is 82% for all datasets and 67% for the validation dataset. Therefore, the developed CNN-based method has better performance than the FFNN-based models.

1. Introduction

Rolling element bearings (REBs) are the most popular source of failure in rotating machinery such as electro fans, induction motors, wind turbines, etc [1, 2]. It is noted that 40 to 50% of

* Corresponding author:
E-mail address: m_behzad@sharif.edu (M. Behzad)

http://dx.doi.org/10.22064/tava.2022.552939.1202

failures in rotating machinery originate from REBs faults [3]. Intelligent fault diagnosis is to apply machine-learning theory such as artificial neural network (ANN), support vector machine (SVM), and deep learning to detect the type of fault in machinery [4-7]. In recent years, intelligent fault diagnosis became more attractive and received attention from academic and industrial researchers and became more useful for fault diagnosis of rotating machinery [8] therefore this highlight, developed machine learning widely [4, 5, 9, 10]. Deep learning is one of the best methods in machine learning and artificial intelligence that has characteristics such as automatic feature extraction, transferability, and best-in-class performance [11, 12]. In addition to deep learning, feed-forward neural networks (FFNNs) have been employed in condition monitoring and diagnosis [13, 14]. Deep learning has better accuracy, is robust to noise, and deals the overfitting better [12]. However, the ANNs have a lower computational cost [5]. The principle of ANNs training is based on error back propagation [15]. Increasing the number of layers in the FFNNs leads to increasing the overfitting and vanishing of gradient during training [16, 17]. Although deep learning originally was used for image classification [18], these days, it is widely employed for many applications, including machinery diagnosis.

Frequency spectrum analysis is currently used to detect and determine fault existence [19]. However, the time-domain analysis is also employed for this purpose. Using frequency domain signal has limitations such as loss frequency of REBs fault frequency harmonics in the spectrum [20, 21]. A minor discrepancy in calculated REBs fault frequency by geometrical method [22], and existing fault frequency in the spectrum (around 1-2 percent) [23, 24]. Some defects such as lubrication problems do not exist in the frequency spectrum [25]. Background noise in the temporal signal is one of the limitations of diagnosis from the raw temporal signals. Time-frequency domain also become a more popular subject for researchers in recent years [26, 27]. Besides the vibration signals, acoustic signals are also used for fault detection of REBs and other structures [28-31].

In one study, Samanta et al. [32] used three optimized ANNs and extracted features from the time-domain signal to detect the faults of the pump. Their results show that the features and classifiers in the detection of the machine condition are effective. In addition, Samanta et al. [33] utilized time-domain features for REBs fault detection. Their method was based on feature extraction by ANN and SVM. The classifier parameters such as kernel parameter for SVM and number of nodes in ANN hidden layer are optimized with particle swarm optimization (PSO). They achieve high classification accuracy by using PSO for optimization. Zhang et al. [34] used a dataset on REBs accelerated-life test published by the center for intelligent maintenance system (IMS) at the University of Cincinnati [35] and a dataset of seeded-fault test on REBs published by Case-western Reserve University (CWRU) [36] and applied deep neural networks (DNN) to RER fault detection. The input of their model is a time-domain signal. In their method, temporal coherence is taken into consideration. This is considered to be an advantage for prognostics. Wang et al. [37] used an enhanced kurtogram for the diagnosis of REBs. The innovation of their study is kurtosis values calculated based on the power spectrum of the envelope signal. Signals were extracted from wavelet packet nodes at different depths. Shen et al. [38] used a fast and adaptive varying-scale morphological analysis for REBs diagnosis. They showed that their method identifies the cause of REBs defects even if the faulty impulses were partially covered by background noise. Saravanan et al. [39] employed the discrete wavelet transform (DWT) for feature extraction and used an ANN for classification. They showed that their method is reliable for the diagnosis of the gearbox in different conditions. In addition, rule-based methods and

signal processing techniques are used for the diagnosis of REBs [40-42]. In the literature, features such as mean, median, kurtosis, peak to peak, minimum and maximum of the signal, standard deviation, absolute mean, skewness, and crest factor are also used to describe the condition of REBs [43, 44]. These methods rely on hand-crafted time-consuming preprocessing of data. Some studies proposed that the classifier should have the ability to classify the data from the raw signal directly, without manual feature extraction in order to use all the information included in the signal [11, 45].

The Convolutional neural networks (CNN) models such as AlexNet [46], LeNet-5 [47], GoogLeNet [48], VGGNet [49], are widely used for classification such as image classification [50] and diagnosis in recent years. The CNN models have a good capacity for noise removal [51].

In one study in the field of REBs diagnosis, Pham et al. [52] implemented the CNN and vibration spectrogram in variable speed conditions of the shaft for fault detection. In their proposed method, vibration signals are represented by spectrograms to apply deep learning methods through preprocessing, using a short-time Fourier transform (STFT). Then, feature extraction and health status classification are performed by a CNN, VGG16. Their model can achieve high accuracy in the diagnosis of REBs. Wen et al. [53] used a data-driven method based on CNN for fault detection. they tested the proposed method on three datasets, including the motor REBs dataset, self-priming centrifugal pump dataset, and axial piston hydraulic pump dataset. they achieved high prediction accuracy for these purposes. Zhang et al. [54] developed a model based on CNN for REBs diagnosis in which the input of the model is a vibration signal. The novelty of their study is transforming the 1D signal into a 2D image. Their CNN-based model has better performance on the 2D image. Deep learning method such as CNN needs a large size dataset for training. Plakias et al. [55] proposed the attentive dense CNN to overcome this drawback of the deep learning method in needing a large amount of dataset. Their method considers the temporal coherence of the data sample by the combination of dense convolutional blocks with an attention mechanism. Jia et al. [56] proposed a method based on the DNN and auto-encoder (AE) for the diagnosis of REBs and planetary gearboxes. Their method consists of pre-training for the training of AE and fine-tuning for tuning all parameters of DNN. In their method the raw data needed to be transformed into the frequency spectra. Li et al. [57] proposed a 3-layer DNN based on the deep belief network for the diagnosis of REBs. In their REB experiments, the fault was created by grooving, so the fault features were completely obvious and their method may not be efficient for smaller types of REBs faults. Wang et al. [58] proposed the four-layer batch-stack AE. In their model, the frequency spectra of temporal signals are used as the input of the model. They achieve better performance with a small number of training epochs. Yousef Khodja et al. [59] proposed a method for the classification of REBs faults using the CNN and the vibration spectrum imaging. In their method, the normalized amplitudes of the spectral content extracted from segmented temporal signals were transformed into spectral images. Time-moving segmentation window is used for this purpose. The spectral images are used as input of the CNN for training and testing.

According to the literature, in addition to the frequency domain and time-frequency domain, the temporal signals are also used for the diagnosis of REBs. In the field of using the temporal signal for diagnosis, some studies used the preprocessing technique to achieve better accuracy. The

mentioned studies used limited REBs datasets. In these cases, overfitting is possible to happen when the models are trained and tested on the small size of the datasets.

The aim of this study is automatic detection of REBs fault existence in the raw temporal signals. In this regard, a new model based on the CNN is developed. The performance of this model is compared with that of a two-layer FFNN and a deep FFNN. The REB run-to-failure dataset used here is collected from a developed experimental setup at Sharif university of technology. In the developed model, no feature extraction step exists and the raw signals are fed to the models. The model is aimed to the detect existence of the impact pattern in the signal generated by faulty REBs. This novel approach introduced in this paper does not use the REBs fault frequencies. To increase the accuracy of the model, the datasets are normalized and used as the inputs of the model. Another advantage of the proposed method is that it does not use any preprocessing technique on the raw temporal signal. for training and testing, 8 run-to-failure test datasets are used that prevent the algorithms from overfitting on a single dataset.

2. Representation of data and experimental setup

2.1. Representation of developed experimental setup

A set of accelerated-life tests on REBs was designed and performed in the condition monitoring lab of the Sharif University of Technology for this research. The test-rig is shown in figure 1. A test REB is mounted on the test-rig at one end of the shaft. Two larger REBs also support the shaft. The shaft is coupled to a 10 kW AC electromotor through the pulley and belt mechanism as the driver system. The pulley ratio is 1.9 which increases the output torque of the motor as well as reduces the speed. The test REB is a 6907 deep groove single-row REBs. The loading system pulls the housing of the test REB downward. Therefore, the loading zone is located at the top of the test REB. Experiments were conducted in constant operating conditions, including 2000 rpm rotational speed and 9000 N radial load. On this platform, an accelerometer is installed vertically on the housing of the test REB (close to the load zone). The sampling frequency for the acceleration measurement is 25.6 kHz. The stopping criterion or failure threshold was defined on the amplitude of the acceleration signal. Therefore, touching the amplitude of 20g was the final failure criterion, and accelerated life tests were stopped at this point.

Fig. 1. Test-rig of accelerated-life tests on REBs.

Eight run-to-failure tests were conducted in the described test-rig, and corresponding vibration data were recorded. At the end of each test, the test REB was disassembled, and final failures

were recognized through visual inspection (figure 2). Table 1 reports the useful life of each test REB and the corresponding verified failure mode at the end of the tests.

Table 1. Summary of accelerated life tests.

Test No.	Failure Mode	Useful life (sec)
1	Rolling element	13704
2	Rolling element	9546
3	Rolling element	10051
4	Inner race	14742
5	Inner race	11670
6	Inner race	26294
7	Rolling element	306610
8	Rolling element	30205

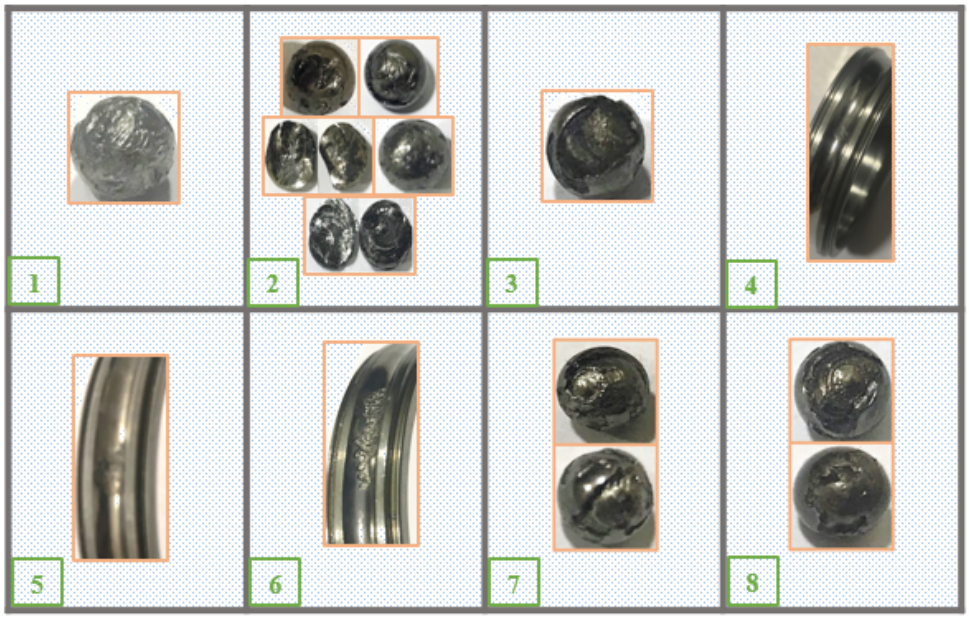

Fig. 2. Visual inspection results of failures in the elements of accelerated-life test REBs.

2.2. Data representation

The aim of this study is the classification of vibration signals corresponding to the defective REBs and the healthy REBs. Label 1 is selected for defective REBs and label 0 is selected for healthy ones. Two samples of defected REB vibration signal and healthy REB signal are depicted in figure 3. There are impact shapes in the defected REB signal that refer to fault existence. The impacts are resulting from the ball passing on defects or striking the ball defect to other REBs elements. The developing model in this study is aimed to detect this pattern.

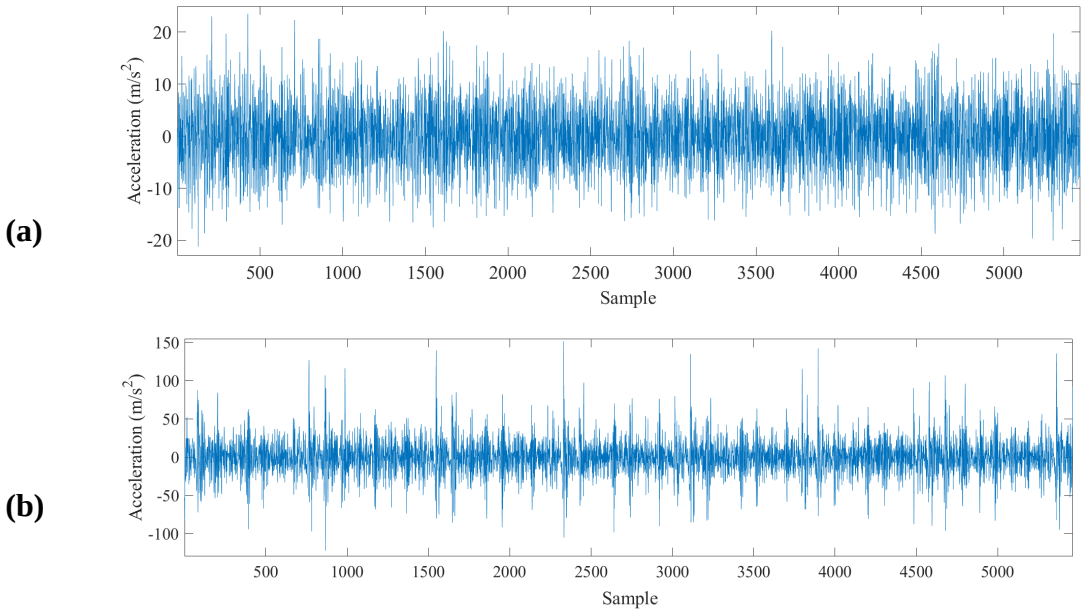

Fig. 3: (a) healthy REB signal example, (b) defective REB signal example

To detect fault initiation in the test REB, the trend of the vibration signal root mean square (RMS) is used. The formula of RMS is represented by equation 1 [60]:

$$X_{RMS} = \sqrt{\frac{1}{N}\sum_{z=1}^{N}|X_z|^2} \quad (1)$$

where the N is the number of samples and X_z is the amplitude of a sample with index z. Figure 4, represented the trend of signals RMS for all tests. Besides the trend study, all selected signals were investigated individually to ensure if the impact pattern exists in the faulty labeled signals. In some cases, the signal RMS has a considerable value but there is no impact pattern in the signal related to the REBs fault. These cases refer to other machine faults.

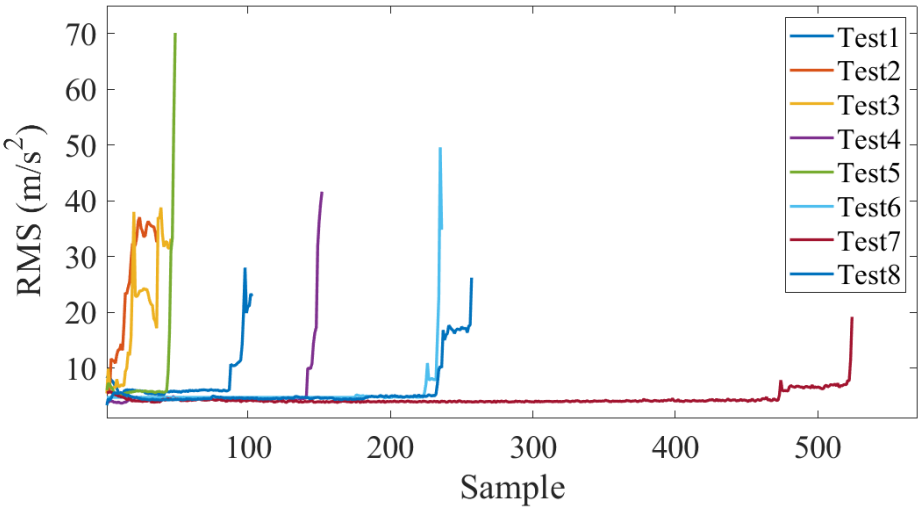

Fig.4: The trend of RMS for all run-to-failure tests

A set of faulty signals (label=1) as well as a set of healthy condition signals (label=0) were selected randomly from eight run-to-failure tests depicted in figure 4. These temporal signals and labels are employed for training and testing the developed models. The inputs of all models are a matrix containing the normalized signals with a similar size and the outputs of all models are 1 or 0 that are predefined before the training of the models. The RMS trend increase and the existence of impact pattern in the signal are two criteria for selecting the faulty signals in this study. The faults created in the REBs are due to spalling [61-63].

3. Development of the new fault detection model

The developed algorithms are aimed to detect impact patterns in the raw vibration signals. The developed CNN-based model consists of four convolutional layers for effective feature extraction and three fully-connected (dense) layer for classification as shown in figure 6. For avoiding the overfitting in the CNN, the dropout process is used. To this aim, each convolution feature map activation is dropped out independently [64]. This process results in regularization and decreasing generalization errors in networks. To transfer the outputs of the network into probabilistic space, the softmax function is selected in the outputs of the fully-connected layer. Equation 2 represents the softmax activation function which computes the probability ($P(x_i)$) of belonging a signal to a class. In this model, the convolutional layers extract the feature of the impact pattern efficiently. The leaky Rectified Linear Unit (Leaky ReLU) is used instead of simple ReLU. Because in some cases, there is no gradient flow in simple ReLU, and also the outputs of the simple ReLU in some cases are zero [65].

$$P(x_i) = \frac{x_i}{\sum_{j=1}^{N} e^{x_j}} \quad (i = 1{:}N) \tag{2}$$

where the x_i is the input of a function with the defined index and $P(x_i)$ is the probability of belonging to a class with index i.

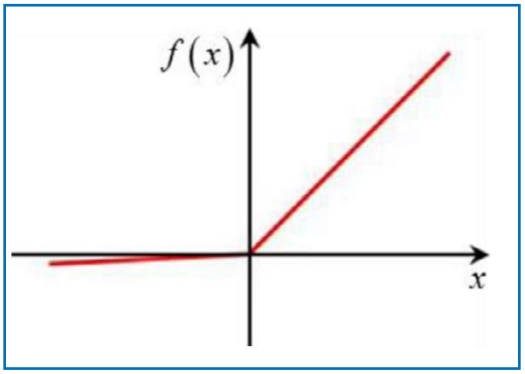

Fig. 5: Leaky ReLU activation function [66]

According to figure 5, the equation of leaky ReLU is represented in equation 3.

$$f(x) = \begin{cases} x & x \geq 0 \\ ax & x < 0 \end{cases} \tag{3}$$

where the parameter a is a trace number. However, the appearance of Leaky ReLU is alike to ReLU. In the convolutional process, the feature of the temporal signal is extracted by the kernel. The kernel is the matrix that moves on the signal such as a window with a certain stride. Every signal is filtered by some of the kernels in every convolutional layer. Through these processes, the features of the signal are extracted. After choosing the appropriate kernel and stride size, the network is ready for training. The max pooling operation is employed to select the maximum value from the feature map region covered by the filter.

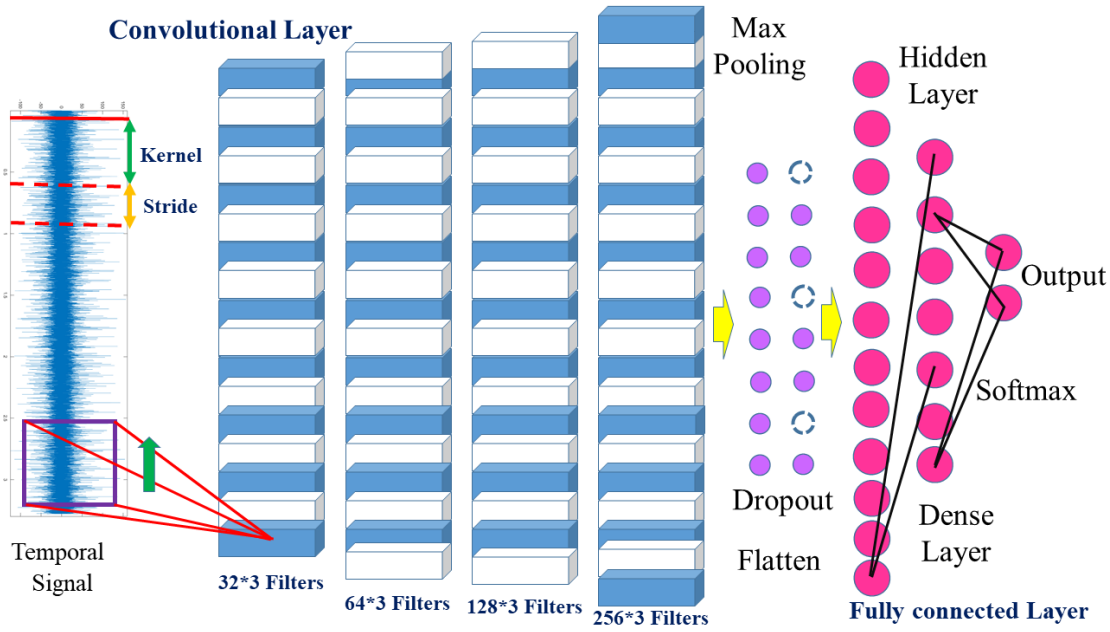

Fig 6: The developed CNN-based model for fault detection in REBs

In this study, the results and accuracy of the CNN-based developed model, the two-layer FFNN, and the deep FFNN are compared (figure 7). The two-layer FFNN is mentioned as a shallow neural network. For better training of the networks, the data are normalized in [-1 1] intervals. In this case, the mean of the signal is changed. However, the schematics of signals are saved and the signal is mapped into a smaller space. In the FFNN, the sigmoid activation function (equation 4) is used. No filters are exerted on signals. The aim is fault detection directly from the raw temporal signals using the AI method. The impact is going to be detected from the raw temporal signals. In this regard, the good capacity for noise removal of CNN is useful.

$$sigmoid(E_i) = O_i = \frac{1}{1 + \exp(-E_i)} \tag{4}$$

where the O_i is the ith output and the E_i is the linear activation of the ith neuron. The inputs of the FFNN models are the raw signal elements. In another word, the input of every neuron in the

input layer is a sample of the temporal signal. The feature extraction by this network is done by non-linear computation training. One of the innovations of this study is converting the high dimensional inputs to the low dimensional outputs (two classes including 0 and 1). It is worthy to emphasize that in actual industrial cases, the faulty REB should be replaced regardless to the type of fault location. The capability of the developed models in this study is detecting the fault existence and it is enough for industrial application. The important advantage of this approach is that there is no need to know the faulty REB code and its fault frequencies.

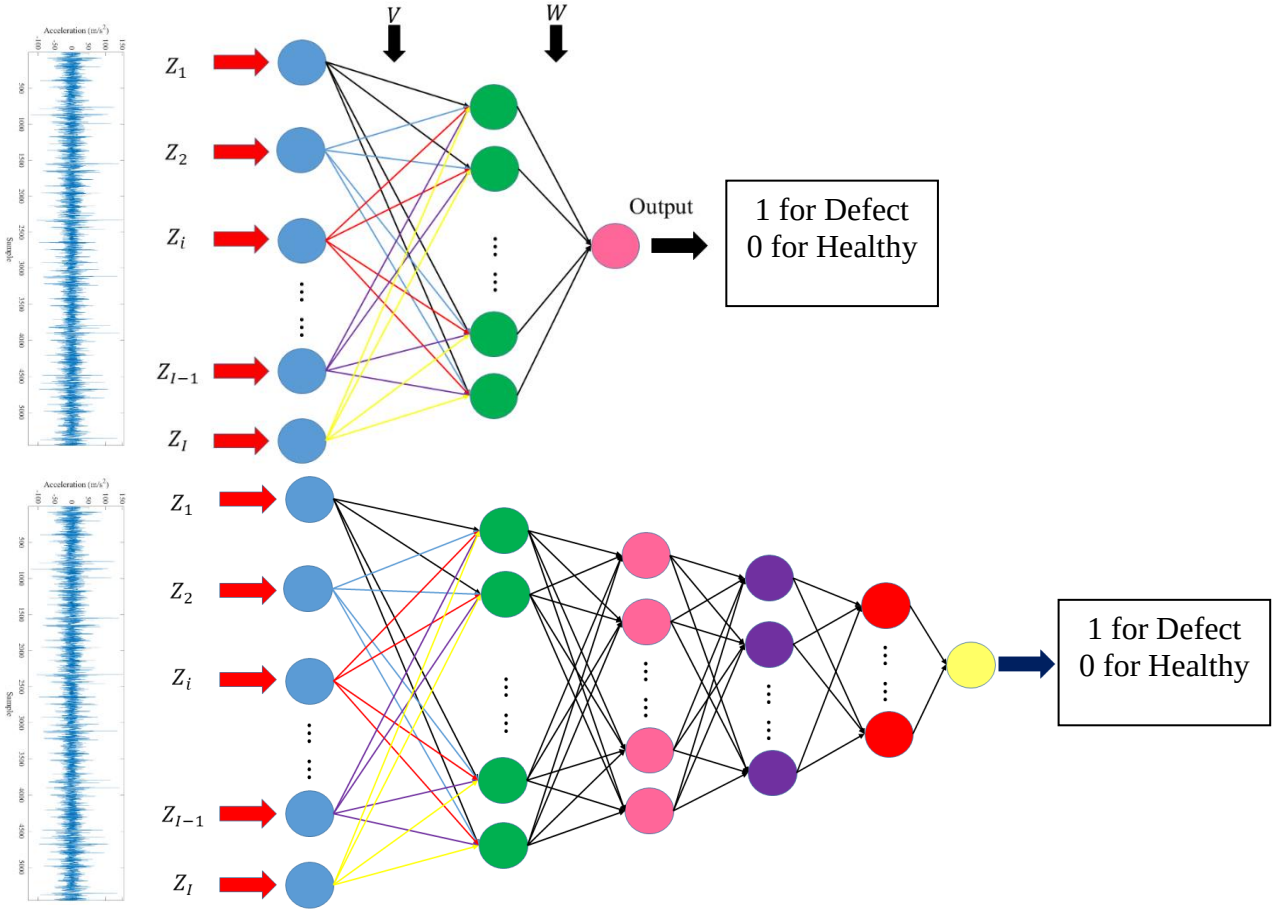

Fig. 7: Two developed FFNNs for classification of the signal with impacts and the healthy signals

(a) The two-layer (shallow) FFNN; (b) The deep FFNN model

In equation 4, if the E_i has a large value, the O_i is equal to 1 for any type of input. This makes a great error in the classification. Therefore, the datasets should be normalized. Normalizing the dataset prevents the models to overfit a certain operating condition. Therefore, the models will not be sensitive to the amplitude of the signal.

4. Results

In this section, the results of implementing the developed algorithms for fault detection of REBs will be expressed and compared.

4.1. Implementing results of two-layer FFNN and deep FFNN

The results of all developed models are totalized and presented after training and testing. The results of the two-layer FFNN are presented in table 2. In the second column, the number of neurons in the hidden layer is presented for several cases. Table 3 describes the results of deep FFNN for several cases. The number of neurons in the second layer to the penultimate layer is presented in the third column from left to right. In this study, the number of layers is referred to the addition of the hidden layers and the output layer.

Table 2: The results of the two-layer FFNN for several cases of neurons in the hidden layer

No.	Number of neurons in hidden layers	Implementing accuracy	No.	Number of neurons in hidden layers	Implementing accuracy
1	10	81.80	9	50	84.80
2	15	83.00	10	55	81.40
3	20	84.90	11	60	84.40
4	25	84.40	12	65	82.20
5	30	83.00	13	70	84.80
6	35	82.70	14	75	81.30
7	40	82.00	**15**	**76**	**85.90**
8	45	81.60	16	80	85.20

Table 3: The results of the deep FFNN for several cases of the hidden layer

No.	Number of layers	Number of neurons in networks	Implementing accuracy	No.	Number of layers	Number of neurons in networks	Implementing accuracy
1	3	10-10	81.00	11	5	45-25-15-5	80.30
2	3	15-15	81.80	12	5	10-10-10-10	80.10
3	3	30-10	81.60	13	5	45-25-10-5	80.90
4	**3**	**60-10**	**82.10**	14	6	55-25-18-10-5	80.70
5	3	75-10	78.30	15	6	70-35-25-15-7	79.90
6	4	15-15-15	80.60	16	6	70-25-18-10-5	79.10
7	4	20-20-20	80.90	17	6	72-45-25-15-8	80.60
8	4	75-15-4	81.00	18	6	80-35-25-15-7	76.70
9	4	60-20-10	80.80	19	6	20-18-16-14-4	77.30
10	5	55-25-12-6	80.10	20	6	20-18-16-14-6	78.70

According to tables 2 and 3, the accuracy of the two-layer FFNN and the deep FFNN for detection of the healthy or unhealthy are 85% and 82%, respectively. Figure 8 shows the confusion matrix for the best accuracy of the two-layer networks with 76 neurons in the hidden layer. According to this figure, the accuracy of validation is 74%. MATLAB is used for implementing the two-layer and the deep networks. 70% of the dataset is used for training, 15% for validation, and 15% for the test. Increasing the number of the hidden layers in the FFNN leads to the training of background noise of signal by networks instead of all prominent features in the time signal. Because in this case, the background noise of the signal is recognized by networks and this is not desired in this case.

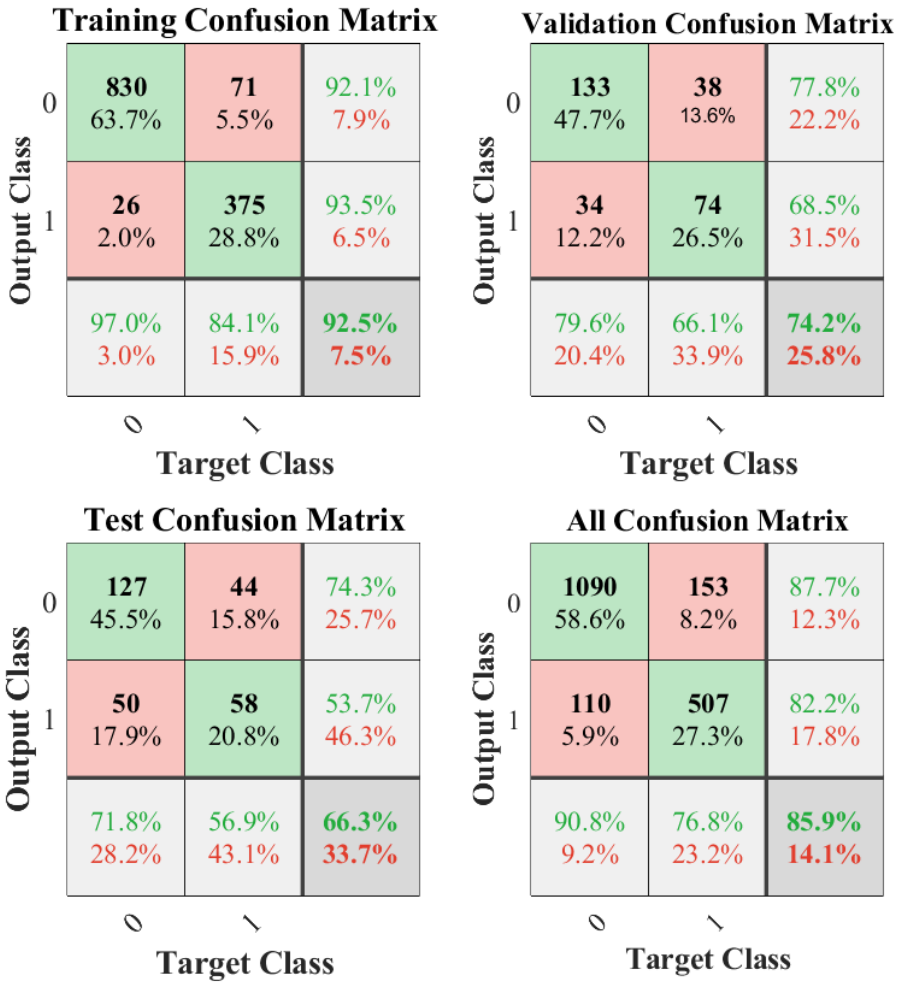

Fig. 8: The confusion matrix of the best accuracy of two-layer FFNN (item 15 in Table 2)

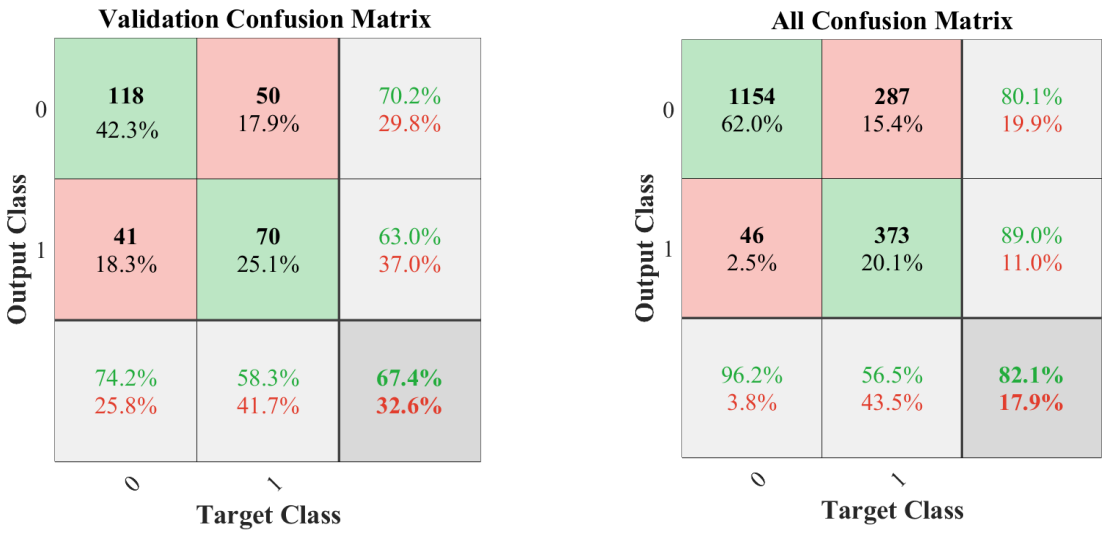

Fig. 9: The confusion matrix of the best accuracy of the deep FFNN (item 4 in Table 3)

4.2. Implementing results of the developed model based on CNN.

The CNN-based model and the FFNN models were implemented on the datasets and the results are presented. Python (programming) is used for implementing the developed CNN-based model. Figure 10, shows the confusion matrix for all datasets and changing accuracy in terms of training epochs. The results show that the accuracy of implementing the developed model is far greater than FFNN models. This is because of efficient feature extraction by the developed model. In this study, 75% of the datasets are used for training and the remaining are used for validation and test of the model. If there is enough dataset for training and testing, it is recommended to use 60 to 80 percent of the dataset for training, and the remaining for validation and testing [16, 67]. The variation of the loss function in terms of training epochs for the CCN-based developed model is presented in figure 11.

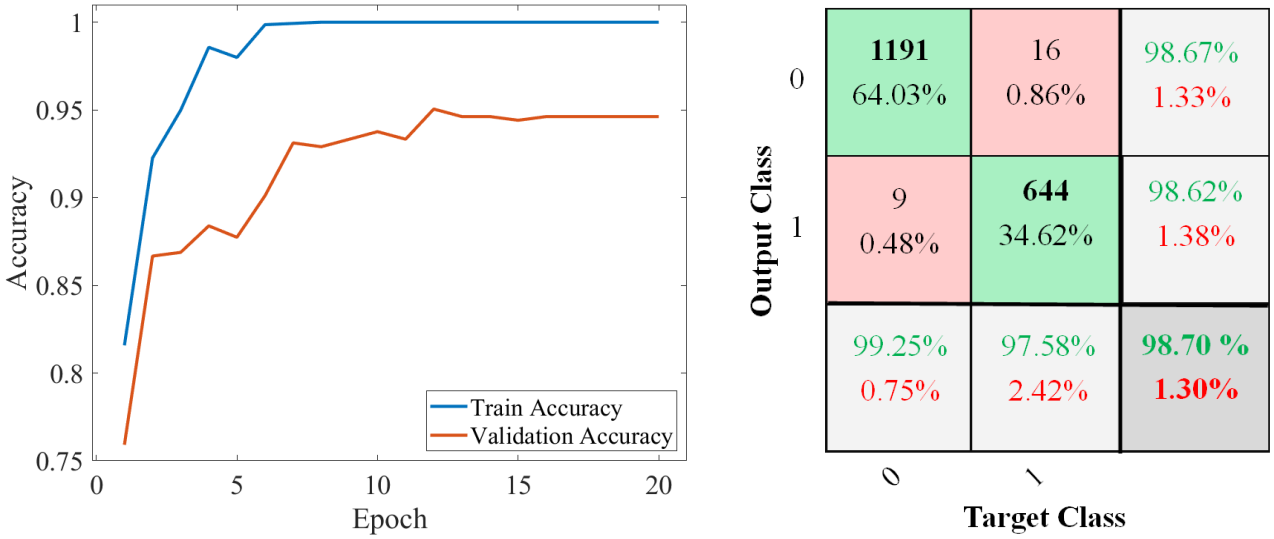

Fig. 10: Changing accuracy in terms of training epochs and confusion matrix for all datasets for the developed CNN-based model

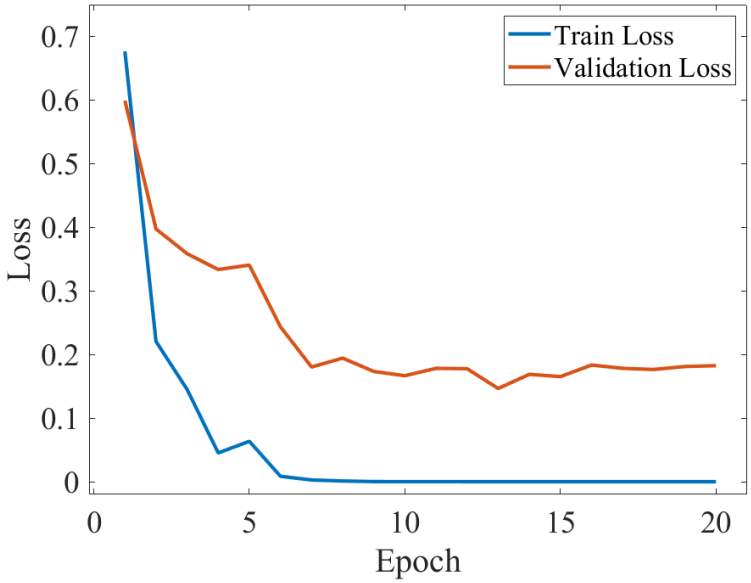

Fig. 11: changing loss function in terms of training epochs for the developed CNN-based model

Normally, the loss function of the validation data has a larger amount than the training data [15]. Also, this is shown in other research areas in the field of using CNN [68]. For the present study, the loss function of the validation data has a larger amount than the training data and this is shown in figure 11. That is because the validation data do not play role in tuning the weight parameters in the training process.

4.3. Discussion and comparison of the developed models

According to results obtained with all methods, the developed CNN-based model has better accuracy. This is because of the automatic and efficient feature extraction in this model. In addition, the two-layer networks have better accuracy than the deep FFNNs. Increasing the layer from the optimized number of layers leads to overfitting of training data and therefore the accuracy of the model is decreased. Increasing the layers leads to training of background noise of signal by networks. This matter leads to a decrease in accuracy in the validation datasets. Certainly, in this case, the complexity of networks is increased. The high accuracy of the CNN-based model is referred to high resistance to overfitting and noise in the signals and sensitivity to the position of the impacts. High accuracy in test and validation datasets refers to this subject. The loss function in figure 11 indicates the correct training, test, and validation. In this study, the number of healthy REBs signals is more than defected REBs. The results indicate that the employed AI techniques for detection of impact patterns in the signal are useful. The dropout process in the CNN-based model is very effective and improves performance. With the normalization of data, the schematic of the signal and impacts in the signal were saved. Unlike deep FFNN, CNN is not sensitive to noise in the background of the signals.

5. Conclusion

In this study, a new method based on the CNN and two FFNN-based models were developed and the performance of the three models were studied and compared. The main capability of the developed models is detecting impact patterns (due to REBs defects) in the raw temporal signal.

The accuracy of methods is compared together. The accuracy of the developed CNN-based model in fault detection of the REBs was 98.6%. Whereas the accuracy of the two-layer FFNN is 85% and that of the deep FFNN is 82%. High accuracy of the CNN-based model is referred to the efficient and automatic feature extraction and high resistance to overfitting and noise in the signals and sensitivity to the position of the impacts. It is obtained that the correct selection of model parameters affects the final accuracy.

The prominent advantage of the developed models in this study is that they do not use the fault frequencies of the REBs. And, they only seek for impact patterns generated by local faults. Since in many industrial applications, detailed information about REBs is unknown to the condition monitoring team, the mentioned advantage is very helpful for automatic intelligent fault detection and interpretation of the signals.

6. Conflicts of Interest

The authors of this paper declare that they have no conflict of interest in all parts of the study.

References

[1] H. Ocak, K.A. Loparo, Estimation of the running speed and bearing defect frequencies of an induction motor from vibration data, Mechanical systems and signal processing, 18 (2004) 515-533.
[2] E.J. Terrell, W.M. Needelman, J.P. Kyle, Wind turbine tribology, in: Green Tribology, Springer, 2012, pp. 483-530.
[3] M. Behzad, S. Feizhoseini, H.A. Arghand, A. Davoodabadi, D. Mba, Failure Threshold Determination of Rolling Element Bearings Using Vibration Fluctuation and Failure Modes, Applied Sciences, 11 (2020) 160.
[4] L. Duan, M. Xie, J. Wang, T. Bai, Deep learning enabled intelligent fault diagnosis: Overview and applications, Journal of Intelligent & Fuzzy Systems, 35 (2018) 5771-5784.
[5] R. Liu, B. Yang, E. Zio, X. Chen, Artificial intelligence for fault diagnosis of rotating machinery: A review, Mechanical Systems and Signal Processing, 108 (2018) 33-47.
[6] K. Patan, J. Korbicz, Artificial neural networks in fault diagnosis, in: Fault Diagnosis, Springer, 2004, pp. 333-379.
[7] A. Widodo, B.-S. Yang, Support vector machine in machine condition monitoring and fault diagnosis, Mechanical systems and signal processing, 21 (2007) 2560-2574.
[8] K. Worden, W.J. Staszewski, J.J. Hensman, Natural computing for mechanical systems research: A tutorial overview, Mechanical Systems and Signal Processing, 25 (2011) 4-111.
[9] S. Khan, T. Yairi, A review on the application of deep learning in system health management, Mechanical Systems and Signal Processing, 107 (2018) 241-265.
[10] R. Zhao, R. Yan, Z. Chen, K. Mao, P. Wang, R.X. Gao, Deep learning and its applications to machine health monitoring, Mechanical Systems and Signal Processing, 115 (2019) 213-237.
[11] Y. Lei, F. Jia, J. Lin, S. Xing, S.X. Ding, An intelligent fault diagnosis method using unsupervised feature learning towards mechanical big data, IEEE Transactions on Industrial Electronics, 63 (2016) 3137-3147.
[12] S. Zhang, S. Zhang, B. Wang, T.G. Habetler, Deep learning algorithms for bearing fault diagnostics—A comprehensive review, IEEE Access, 8 (2020) 29857-29881.
[13] M. Behzad, H.A. Arghand, A. Rohani Bastami, Remaining useful life prediction of ball-bearings based on high-frequency vibration features, Proceedings of the Institution of Mechanical Engineers, Part C: Journal of Mechanical Engineering Science, 232 (2018) 3224-3234.
[14] M.-Y. Chow, P.M. Mangum, S.O. Yee, A neural network approach to real-time condition monitoring of induction motors, IEEE Transactions on industrial electronics, 38 (1991) 448-453.
[15] S. Haykin, Neural Networks A Comprehensive Foundation, eight ed, in, Pearson Prentice Hall, India, 2009.
[16] Y. Bengio, I. Goodfellow, A. Courville, Deep learning, MIT press Cambridge, MA, USA, 2017.

[17] X. Glorot, Y. Bengio, Understanding the difficulty of training deep feedforward neural networks, in: Proceedings of the thirteenth international conference on artificial intelligence and statistics, JMLR Workshop and Conference Proceedings, 2010, pp. 249-256.
[18] G.E. Hinton, S. Osindero, Y.-W. Teh, A fast learning algorithm for deep belief nets, Neural computation, 18 (2006) 1527-1554.
[19] S.J. Lacey, An overview of bearing vibration analysis, Maintenance & asset management, 23 (2008) 32-42.
[20] M. Behzad, A. Kiakojouri, H.A. Arghand, A. Davoodabadi, Inaccessible rolling bearing diagnosis using a novel criterion for Morlet wavelet optimization, Journal of Vibration and Control, 28 (2022) 1239-1250.
[21] A. Hu, L. Xiang, S. Xu, J. Lin, Frequency loss and recovery in rolling bearing fault detection, Chinese Journal of Mechanical Engineering, 32 (2019) 1-12.
[22] D.S. Shah, V.N. Patel, A review of dynamic modeling and fault identifications methods for rolling element bearing, Procedia Technology, 14 (2014) 447-456.
[23] O. Janssens, V. Slavkovikj, B. Vervisch, K. Stockman, M. Loccufier, S. Verstockt, R. Van de Walle, S. Van Hoecke, Convolutional neural network based fault detection for rotating machinery, Journal of Sound and Vibration, 377 (2016) 331-345.
[24] W.A. Smith, R.B. Randall, Rolling element bearing diagnostics using the Case Western Reserve University data: A benchmark study, Mechanical systems and signal processing, 64 (2015) 100-131.
[25] P. Boškoski, J. Petrovčič, B. Musizza, Đ. Juričić, Detection of lubrication starved bearings in electrical motors by means of vibration analysis, Tribology international, 43 (2010) 1683-1692.
[26] Z. Feng, M. Liang, F. Chu, Recent advances in time–frequency analysis methods for machinery fault diagnosis: A review with application examples, Mechanical Systems and Signal Processing, 38 (2013) 165-205.
[27] G. Yu, A concentrated time–frequency analysis tool for bearing fault diagnosis, IEEE Transactions on Instrumentation and Measurement, 69 (2019) 371-381.
[28] A. Anwarsha, T. Narendiranath Babu, Recent advancements of signal processing and artificial intelligence in the fault detection of rolling element bearings: a review, Journal of Vibroengineering, 24 (2022).
[29] K. Rahmatnezhad, M. Zarastvand, R. Talebitooti, Mechanism study and power transmission feature of acoustically stimulated and thermally loaded composite shell structures with double curvature, Composite Structures, 276 (2021) 114557.
[30] M. Zarastvand, M. Asadijafari, R. Talebitooti, Improvement of the low-frequency sound insulation of the poroelastic aerospace constructions considering Pasternak elastic foundation, Aerospace Science and Technology, 112 (2021) 106620.
[31] M. Zarastvand, M. Asadijafari, R. Talebitooti, Acoustic wave transmission characteristics of stiffened composite shell systems with double curvature, Composite Structures, 292 (2022) 115688.
[32] B. Samanta, K. Al-Balushi, S. Al-Araimi, Artificial neural networks and support vector machines with genetic algorithm for bearing fault detection, Engineering applications of artificial intelligence, 16 (2003) 657-665.
[33] B. Samanta, C. Nataraj, Use of particle swarm optimization for machinery fault detection, Engineering Applications of Artificial Intelligence, 22 (2009) 308-316.
[34] R. Zhang, Z. Peng, L. Wu, B. Yao, Y. Guan, Fault diagnosis from raw sensor data using deep neural networks considering temporal coherence, Sensors, 17 (2017) 549.
[35] H. Qiu, J. Lee, J. Lin, G. Yu, Robust performance degradation assessment methods for enhanced rolling element bearing prognostics, Advanced Engineering Informatics, 17 (2003) 127-140.
[36] D. Neupane, J. Seok, Bearing fault detection and diagnosis using case western reserve university dataset with deep learning approaches: A review, IEEE Access, 8 (2020) 93155-93178.
[37] D. Wang, W.T. Peter, K.L. Tsui, An enhanced Kurtogram method for fault diagnosis of rolling element bearings, Mechanical Systems and Signal Processing, 35 (2013) 176-199.
[38] C. Shen, Q. He, F. Kong, P.W. Tse, A fast and adaptive varying-scale morphological analysis method for rolling element bearing fault diagnosis, Proceedings of the Institution of Mechanical Engineers, Part C: Journal of Mechanical Engineering Science, 227 (2013) 1362-1370.
[39] N. Saravanan, K. Ramachandran, Incipient gear box fault diagnosis using discrete wavelet transform (DWT) for feature extraction and classification using artificial neural network (ANN), Expert systems with applications, 37 (2010) 4168-4181.
[40] I. Attoui, N. Boutasseta, N. Fergani, B. Oudjani, A. Deliou, Vibration-based bearing fault diagnosis by an integrated DWT-FFT approach and an adaptive neuro-fuzzy inference system, in: 2015 3rd International Conference on Control, Engineering & Information Technology (CEIT), IEEE, 2015, pp. 1-6.

[41] P. Gupta, M. Pradhan, Fault detection analysis in rolling element bearing: A review, Materials Today: Proceedings, 4 (2017) 2085-2094.
[42] Z. Yang, U.C. Merrild, M.T. Runge, G. Pedersen, H. Børsting, A study of rolling-element bearing fault diagnosis using motor's vibration and current signatures, IFAC Proceedings Volumes, 42 (2009) 354-359.
[43] G.E. Kondhalkar, G. Diwakar, Crest factor measurement by experimental vibration analysis for preventive maintenance of bearing, in: International Conference on Reliability, Risk Maintenance and Engineering Management, Springer, 2019, pp. 133-138.
[44] H. Shao, H. Jiang, X. Zhang, M. Niu, Rolling bearing fault diagnosis using an optimization deep belief network, Measurement Science and Technology, 26 (2015) 115002.
[45] T. Ince, S. Kiranyaz, L. Eren, M. Askar, M. Gabbouj, Real-time motor fault detection by 1-D convolutional neural networks, IEEE Transactions on Industrial Electronics, 63 (2016) 7067-7075.
[46] A. Krizhevsky, I. Sutskever, G.E. Hinton, Imagenet classification with deep convolutional neural networks, Advances in neural information processing systems, 25 (2012).
[47] Y. LeCun, LeNet-5, convolutional neural networks, URL: http://yann. lecun. com/exdb/lenet, 20 (2015) 14.
[48] C. Szegedy, W. Liu, Y. Jia, P. Sermanet, S. Reed, D. Anguelov, D. Erhan, V. Vanhoucke, A. Rabinovich, Going deeper with convolutions, in: Proceedings of the IEEE conference on computer vision and pattern recognition, 2015, pp. 1-9.
[49] K. Simonyan, A. Zisserman, Very deep convolutional networks for large-scale image recognition, arXiv preprint arXiv:1409.1556, (2014).
[50] K. O'Shea, R. Nash, An introduction to convolutional neural networks, arXiv preprint arXiv:1511.08458, (2015).
[51] C. Lu, Z. Wang, B. Zhou, Intelligent fault diagnosis of rolling bearing using hierarchical convolutional network based health state classification, Advanced Engineering Informatics, 32 (2017) 139-151.
[52] M.T. Pham, J.-M. Kim, C.H. Kim, Accurate bearing fault diagnosis under variable shaft speed using convolutional neural networks and vibration spectrogram, Applied Sciences, 10 (2020) 6385.
[53] L. Wen, X. Li, L. Gao, Y. Zhang, A new convolutional neural network-based data-driven fault diagnosis method, IEEE Transactions on Industrial Electronics, 65 (2017) 5990-5998.
[54] W. Zhang, G. Peng, C. Li, Bearings fault diagnosis based on convolutional neural networks with 2-D representation of vibration signals as input, in: MATEC web of conferences, EDP Sciences, 2017, pp. 13001.
[55] S. Plakias, Y.S. Boutalis, Fault detection and identification of rolling element bearings with Attentive Dense CNN, Neurocomputing, 405 (2020) 208-217.
[56] F. Jia, Y. Lei, J. Lin, X. Zhou, N. Lu, Deep neural networks: A promising tool for fault characteristic mining and intelligent diagnosis of rotating machinery with massive data, Mechanical systems and signal processing, 72 (2016) 303-315.
[57] W. Li, W. Shan, X. Zeng, Bearing fault identification based on deep belief network, Journal of vibration engineering, 29 (2016) 340-347.
[58] J. Wang, S. Li, Z. An, X. Jiang, W. Qian, S. Ji, Batch-normalized deep neural networks for achieving fast intelligent fault diagnosis of machines, Neurocomputing, 329 (2019) 53-65.
[59] A. Youcef Khodja, N. Guersi, M.N. Saadi, N. Boutasseta, Rolling element bearing fault diagnosis for rotating machinery using vibration spectrum imaging and convolutional neural networks, The International Journal of Advanced Manufacturing Technology, 106 (2020) 1737-1751.
[60] H. Ahmed, A.K. Nandi, Condition monitoring with vibration signals: Compressive sampling and learning algorithms for rotating machines, John Wiley & Sons, 2020.
[61] M.N. Kotzalas, T.A. Harris, Fatigue failure progression in ball bearings, J. Trib., 123 (2001) 238-242.
[62] K. Mori, N. Kasashima, T. Yoshioka, Y. Ueno, Prediction of spalling on a ball bearing by applying the discrete wavelet transform to vibration signals, Wear, 195 (1996) 162-168.
[63] H. Shi, X. Bai, K. Zhang, Z. Wang, Z. Liu, Spalling localization on the outer ring of hybrid ceramic ball bearings based on the sound signals, IEEE Access, 7 (2019) 134621-134634.
[64] J. Tompson, R. Goroshin, A. Jain, Y. LeCun, C. Bregler, Efficient object localization using convolutional networks, in: Proceedings of the IEEE conference on computer vision and pattern recognition, 2015, pp. 648-656.
[65] M. Wang, S. Lu, D. Zhu, J. Lin, Z. Wang, A high-speed and low-complexity architecture for softmax function in deep learning, in: 2018 IEEE Asia Pacific Conference on Circuits and Systems (APCCAS), IEEE, 2018, pp. 223-226.
[66] Y. Liu, X. Wang, L. Wang, D. Liu, A modified leaky ReLU scheme (MLRS) for topology optimization with multiple materials, Applied Mathematics and Computation, 352 (2019) 188-204.

[67] I. Guyon, A scaling law for the validation-set training-set size ratio, AT&T Bell Laboratories, 1 (1997).
[68] A.A. Pol, G. Cerminara, C. Germain, M. Pierini, A. Seth, Detector monitoring with artificial neural networks at the CMS experiment at the CERN Large Hadron Collider, Computing and Software for Big Science, 3 (2019) 1-13.